ELSEVIER

Biochemical Engineering Journal 40 (2008) 408–414

Biochemical Engineering Journal

www.elsevier.com/locate/bej

Preparation and characterization of carboxyl functionalization of chitosan derivative magnetic nanoparticles

Gui-yin Li [a,b], Ke-long Huang [a], Yu-ren Jiang [a], Ping Ding [a], Dong-liang Yang [b,*]

[a] College of Chemistry and Chemical Engineering, Central South University, Changsha 410083, China
[b] Hunan Vocational College of Science and Technology, Changsha 410004, China

Received 20 May 2007; received in revised form 22 December 2007; accepted 7 January 2008

Abstract

The functionalized magnetic Fe_3O_4-chitosan derivative nanoparticles have been prepared by the covalent binding of alpha-ketoglutaric acid chitosan (KCTS) onto the surface of Fe_3O_4 magnetic nanoparticles via carbodiimide activation. Transmission electron microscopy (TEM) showed that the KCTS-bound Fe_3O_4 nanoparticles were regular spheres with a mean diameter of 26 nm. X-ray diffraction (XRD) patterns indicated that the Fe_3O_4 nanoparticles were pure Fe_3O_4 with a spinel structure, and the binding of KCTS did not result in a phase change. The binding of KCTS to the Fe_3O_4 nanoparticles was also demonstrated by the measurement of thermogravimetric analysis (TGA), differential scanning calorimetry analysis (DSC) and Fourier transform infrared (FTIR) spectra. Magnetic measurement revealed that the saturated magnetization of the KCTS-bound Fe_3O_4 nanoparticles reached 24.8 emu g^{-1} and the nanoparticles showed the characteristics of superparamagnetism.

Keywords: Nanostructures; Magnetic properties; Transmission electron microscopy (TEM)

1. Introduction

With the rapid development of nanotechnology, magnetic nanoparticles are currently studied widely. Superparamagnetic iron oxide (Fe_3O_4) nanoparticles have attracted researchers from various fields such as physics, medicine, biology, and materials science due to their multifunctional properties such as small size, superparamagnetism, and low toxicity, etc. [1,2]. Several methods have been developed to synthesize magnetic Fe_3O_4 nanoparticles: (1) coprecipitation of ferrous (Fe^{2+}) and ferric (Fe^{3+}) aqueous solution in the presence of a base [3]; (2) thermal decomposition of an iron complex [4]; (3) by a sonochemical approach [5]. However, Fe_3O_4 nanoparticles tend to aggregate due to strong magnetic dipole–dipole attractions between particles. So, stabilizers such as surfactants, oxide or polymeric compounds (especially biocompatible polymer) with some specific functional groups have been used to modify these particles to increase the stability [6–9]. Superparamagnetic Fe_3O_4 nanoparticles coated with polymers are usually composed of the magnetic cores to ensure a strong magnetic response and a polymeric shell to provide favorable functional groups and features, which have various applications in biomedicine fields for diagnostic magnetic resonance imaging [10], drug delivery systems [11], therapeutic regimes [12], cell/enzyme immobilization [13] and so on.

Chitosan, poly(1 → 4)-2-amino-2-deoxy-D-glucan, is a polyaminosaccharide with many significant biological (biodegradable, biocompatible, bioactive) and chemical properties (polycationic, hydrogel, reactive groups such as OH and NH_2). So, chitosan and its derivatives have been widely used in many biomedical fields [14]. As a special functional material, the preparations of magnetic chitosan beads have been attracting the researchers these years [15,16]. However, as the resultant magnetic composites were either aggregated or unstable due to polymer cross-linking or physisorption, and chitosan has no suitable functional groups to bind directly onto Fe_3O_4 nanoparticles, many researchers are looking for various methods to modify chitosan and bind onto Fe_3O_4 particles. Carboxymethylated chitosan-Fe_3O_4 particles have been prepared by the carboxymethylated chitosan and then covalently bound onto Fe_3O_4 nanoparticles via carbodiimide activation [17,18]. Chitosan-poly(acrylic acid) (CS-PAA) polymer magnetic microspheres were prepared by cationic CS

* Corresponding author. Tel.: +86 731 8830827; fax: +86 731 8879850.
E-mail addresses: klhuang@mail.csu.edu.cn (K.-l. Huang), dongliangyang2004@yhoo.com.cn (D.-l. Yang).

1369-703X/$ – see front matter © 2008 Elsevier B.V. All rights reserved.
doi:10.1016/j.bej.2008.01.018

coating negative charged Fe_3O_4 nanoparticles by electrostatic adsorption and subsequent polymerization of acrylic acid (AA) onto the CS-coated Fe_3O_4 cores [19]. These polymer magnetic microspheres had a high Fe_3O_4 loading content, and showed unique pH-dependent behaviors on the size and zeta potential.

More recently, in our group, a kind of chitosan derivatives (KCTS) with carboxyl group were prepared through modifying the chitosan with alpha-ketoglutaric acid, which could be covalently coupled with diverse bioactive macromolecules, enzymes and liposomes [14]. Following our previous work, in this study, we have been prepared Fe_3O_4 magnetic nanoparticles with 20–30 nm by hydrothermal method using H_2O_2 as an oxidizer. Then we successfully prepared the monodisperse KCTS-bound Fe_3O_4 nanoparticles by the covalent binding of KCTS onto Fe_3O_4 nanoparticles via carbodiimide activation. The size, structure, and magnetic properties of the resultant magnetic nanoparticles were characterized by TEM, XRD and vibrating-sample magnetometer (VSM). The binding of KCTS to the magnetic nanoparticles via carbodiimide activation was confirmed by FTIR, TGA and DSC. This information will be useful for further applications of the novel magnetic material in the immobilized enzyme system or removal of metal ions and many other industrial processes.

2. Experiment

2.1. Materials

Chitosan (CTS, MW 4.9×10^5, degree of deacetylation 95%) was procured from Dalian Xindie Chitin Co. Ltd. Alpha-ketoglutaric acid was purchased from Qianshan Science and Technology Development Company, Zhuhai of China. Ferrous sulphates heptahydrate ($FeSO_4 \cdot 7H_2O$) and aqueous ammonia solution ($NH_3 \cdot H_2O$) were purchased from Tianjin No. 3 Chemical Plant. Sodium borohydride ($NaBH_4$) was supplied by Fluka Co. Carbodiimides (cyanamide, CH_2N_2) were supplied from Sigma Chemical Co., Ltd. Other chemicals were of analytic grade and used without further purification. All solutions were prepared with distilled, deionized water.

2.2. Preparation of KCTS

KCTS was prepared according to the method of Ding et al. [14]. CTS (4.5 g) was dissolved in 100 ml 1% acetic acid, and then α-ketoglutaric acid (7.2 g) was added to the polymeric solution. The pH of the solution was adjusted to 4.5–5.0 using sodium hydroxide solution. Afterwards, sodium borohydride was added to the stirred mixture at 37 °C. The pH of the polymeric solution was adjusted to 6.5–7.0 using hydrochloric acid and the mixture were further stirred for 24 h. The reaction was terminated by 95% alcohol; the precipitated polymer was filtered, washed 3–4 times with ethanol and diethyl ether, respectively. The product was dried in an infrared drier. Scheme 1 showed a schematic representation of the preparation of KCTS.

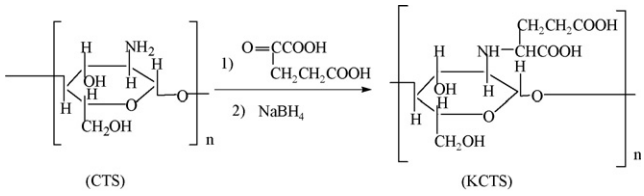

Scheme 1. A reaction scheme for synthesis of KCTS.

2.3. Synthesis of Fe_3O_4 magnetic nanoparticles

Fe_3O_4 nanoparticles were prepared by hydrothermal method with a ferrous complex using H_2O_2 as an oxidizer. Ferrous sulphates heptahydrate (2.502 g) was dissolved in 30 ml water, then 10 ml 50 g l^{-1} PEG-20,000 and 30 ml NH_4OH solution were added to the solution at 30 °C under vigorous stirring. During the reaction process, the pH was maintained at about 10. Afterwards, 0.27 ml 30% H_2O_2 solution was added to the stirred mixture and stirred for 20 min. The mixture was put into the autoclaves and heated at 160 °C for 5 h in a furnace. The Fe_3O_4 nanoparticles were gained after the reaction mixture was separated with a centrifuge at 6000 rpm for 15 min and washed several times with water and ethanol, finally dried in a vacuum oven at 70 °C.

2.4. Preparation of KCTS-bound Fe_3O_4 nanoparticles

Fe_3O_4 nanoparticles (0.2 g) were washed with 99.5% ethanol twice and dispersed in a solution with 30 ml paraffin and 0.5 ml span-80, and then 15.0 ml solution of KCTS in acetic acid with concentration of 2% was added. The suspension was mixed by ultrasonic irradiation for 30 min, and then transferred into a three-necked flask with a mechanical stirrer after adding 1 ml carbodiimide solution (30 g l^{-1} in 0.003 M phosphate buffer, pH 6.0, 1 M NaCl). After 4 h, the KCTS-bound Fe_3O_4 nanoparticles were recovered from the reaction mixture by placing the bottle on a permanent magnet with a surface magnetization of 6000 G. The magnetic particles settled within 1–2 min and then were washed three times with water and ethanol, and finally dried at 50 °C in a vacuum oven.

2.5. Carboxyl group analysis

The number of carboxyl groups in each gram of magnetic microspheres was determined by acid–base titration. To minimize the interference of the magnetite particles, 0.5 g microsphere sample was dialyzed against a 0.050 M ethylenediaminetetraacetic acid disodium salt (EDTA) solution. This treatment led to the dissolution of the magnetite particles leaving a white polymer powder behind. The polymer was rinsed with a 1.0 M acetic acid solution and separated from the supernatant by centrifugation. It was then rinsed with distilled water thrice. The polymer was dried under vacuum, and a weighed amount was titrated with a standardized NaOH solution for acid content.

2.6. Characterizations of KCTS-bound Fe_3O_4 nanoparticles

FTIR spectra of Fe_3O_4 nanoparticles, KCTS and KCTS-bound Fe_3O_4 nanoparticles were recorded with KBr discs in the range of 4000–400 cm^{-1} on Nicolet AVATAR360 Fourier-transfer infrared.

The mean size and size distribution of the magnetic Fe_3O_4 nanoparticles and KCTS-bound Fe_3O_4 nanoparticles were measured by a dynamic laser light scattering (DLS) apparatus (MALVEN, MASTERSIZER 2000, British) in aqueous solution with pH 7.

X-ray diffraction (XRD) measurement: The crystal structure of the iron oxide nanoparticles and KCTS-bound Fe_3O_4 nanoparticles were obtained by the powder XRD pattern of each sample recorded with a Philips D/Max-2500 diffractometer, using a monochromatized X-ray beam with nickel-filtered Cu Kα radiation with 4 min^{-1} scan rate. A continuous scan mode was used to collect 2θ data from 10° to 90°.

Transmission electron microscopy (TEM) measurement: The average particle size, size distribution and morphology of the samples were studied using a H-600 transmission electron microscope. A drop of well dispersed nanoparticle dispersion was placed onto the amorphous carbon-coated 200 mesh copper grid, followed by drying the sample at ambient temperature, before it was loaded into the microscope.

Thermal analysis: Thermogravimetric analysis (TGA) and differential scanning calorimetry analysis (DSC) were carried out for powder samples using a NETZSCHSTA 449C thermogravimetric analyzer. Samples weighing between 5 and 15 mg were heated from 30 to 700 °C at a heating rate of 10 °C min^{-1} in air.

Magnetic measurements: A VSM (JDM-13D magnetometer) was used to characterize the magnetic properties of Fe_3O_4 nanoparticles and KCTS-bound Fe_3O_4 nanoparticles. The hysteresis of the magnetization was obtained by changing H between +4000 and −4000 Oe, these measurements were carried out at 300 K.

3. Results and discussion

3.1. FTIR spectra analysis

The magnetic KCTS-bound Fe_3O_4 nanoparticles were prepared by two steps with suspension cross-linking technique. It is summarized as follows:

(1) The first step is the synthesis of Fe_3O_4 particles by hydrothermal method with a ferrous complex using H_2O_2 as an oxidizer. Scheme 2 showed a schematic representation of the preparation of Fe_3O_4 nanoparticles.
(2) The second one is the binding of KCTS to the Fe_3O_4 nanoparticles. KCTS and Fe_3O_4 aqueous slurry were mixed in appropriate proportion with reverse-phase suspension cross-linking method to form the novel magnetic nanoparticles with carboxyl group. Scheme 3 showed an illustration for the KCTS binding to the Fe_3O_4 nanoparticles.

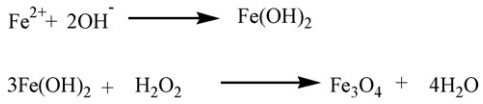

Scheme 2. A schematic representation of the preparation of Fe_3O_4 nanoparticles.

Fig. 1 showed the FTIR spectra of naked Fe_3O_4 (a), KCTS (b) and KCTS-bound Fe_3O_4 nanoparticles (c). The peak around 3440 cm^{-1} observed in curves b and c relates to the –OH group. For the naked Fe_3O_4 (Fig. 1(a)), the peak at 569 cm^{-1} relates to Fe–O group. For the IR spectrum of KCTS (Fig. 1(b)), the characteristic absorption bands appeared at 1612 cm^{-1} which can be assigned to the absorption peaks of the C=O stretching of carboxyl groups of KCTS, peaks 1576 cm^{-1} appeared to N–H bending vibration. In the spectrum of KCTS-bound Fe_3O_4 magnetic nanoparticles (Fig. 1(c)), compared with the spectrum of KCTS, the 1576 cm^{-1} peak of N–H bending vibration shifted to 1561 cm^{-1}, 1612 cm^{-1} peak of the C=O stretching of carboxyl group shifted to 1624 cm^{-1} [19] and a new sharp peak 562 cm^{-1} appeared. The results indicated that KCTS was bound to Fe_3O_4 magnetite nanoparticles successfully. Thus, the binding of KCTS onto the surface of Fe_3O_4 nanoparticles could be illustrated as Scheme 3.

3.2. Particle size and structure of KCTS-bound Fe_3O_4 nanoparticles

The typical TEM micrographs for the Fe_3O_4 nanoparticles and KCTS-bound Fe_3O_4 nanoparticles were shown in Fig. 2. The particles with nanometer size were successfully prepared as shown in the figure. The TEM image of Fe_3O_4 nanoparticles was shown in Fig. 2(a), it was clear that the naked Fe_3O_4 nanoparticles were essentially monodisperse and had a mean diameter of 23 nm. Because the surface of iron oxide with negative charges has an affinity toward KCTS, protonated KCTS could coat the magnetite nanoparticles by the electrostatic interaction. Furthermore, as Scheme 3, KCTS could link with Fe_3O_4

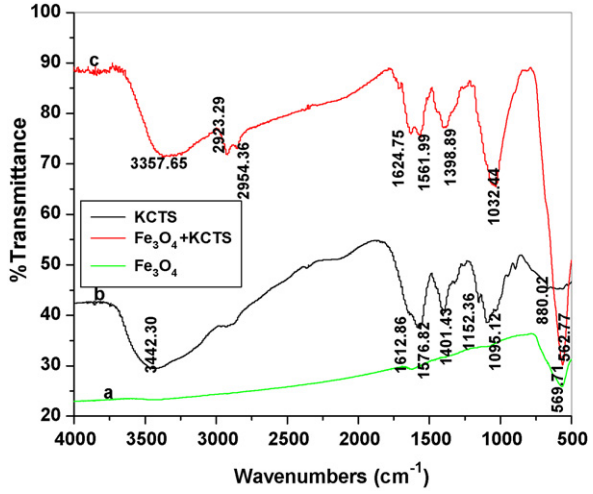

Fig. 1. FTIR of the magnetic Fe_3O_4 particles (a), KCTS (b), KCTS-bound and Fe_3O_4 nanoparticles (c).

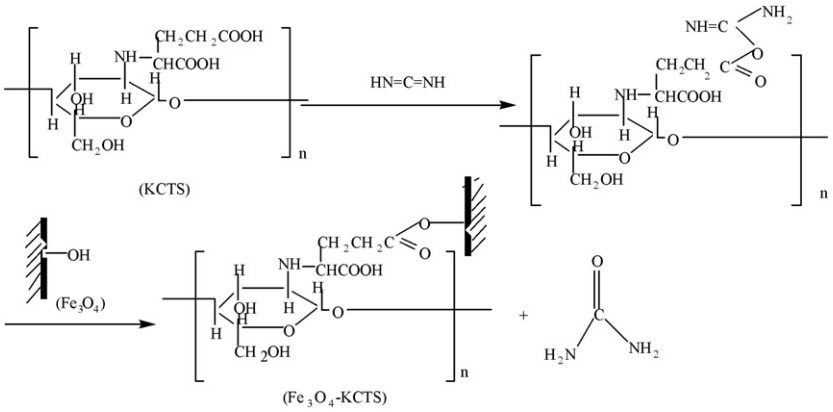

Scheme 3. An illustration for the KCTS binding onto Fe_3O_4 nanoparticles.

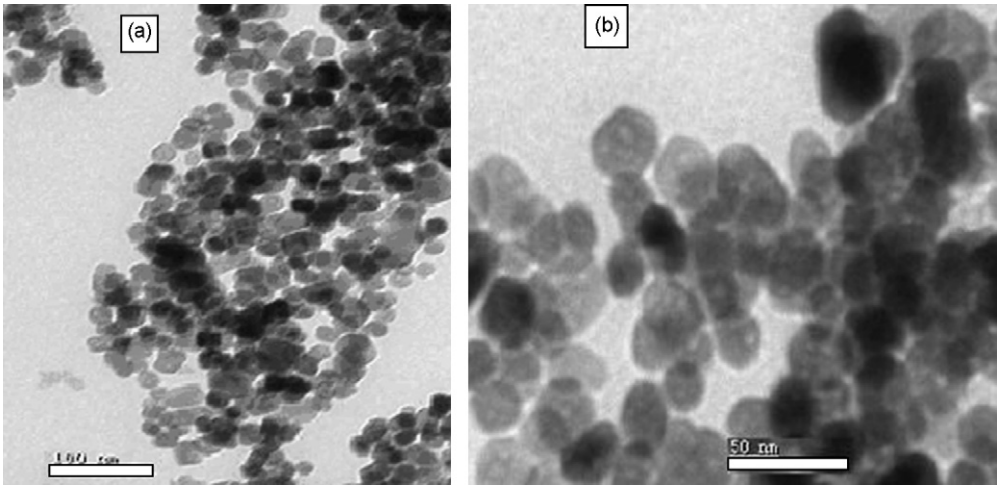

Fig. 2. TEM images of the magnetic Fe_3O_4 particles (a) and KCTS-bound Fe_3O_4 nanoparticles (b).

nanoparticles through carbodiimide activation. The TEM image of KCTS-bound Fe_3O_4 nanoparticles was shown in Fig. 2(b). The KCTS-bound Fe_3O_4 nanoparticles were nearly spherical in shape. The structure of KCTS-bound Fe_3O_4 nanoparticles was looser, leading to the bigger size, the average diameter of such a structure was 26 nm. Size distributions were determined by DLS (Fig. 3) in aqueous solution, the size of the new nanoparticles (Fig. 3(b)) was in the range from 10 to 100 nm, the mean diameter was 52 nm, which was bigger than determined by TEM, presumably arising from the dry state of the TEM measurement.

Fig. 4 showed the XRD patterns for the naked and KCTS-bound Fe_3O_4 nanoparticles. Six characteristic peaks for Fe_3O_4 ($2\theta = 30.1^\circ$, 35.5°, 43.1°, 53.4°, 57.0° and 62.6°) marked by their indices ((2 2 0), (3 1 1), (4 0 0), (4 2 2), (5 1 1) and (4 4 0)) were observed for both samples. These peaks are consistent with the database in JCPDS file (PDF No. 65-3107) and reveal that the resultant nanoparticles were Fe_3O_4. It is explained that the binding process did not result in the phase change of Fe_3O_4.

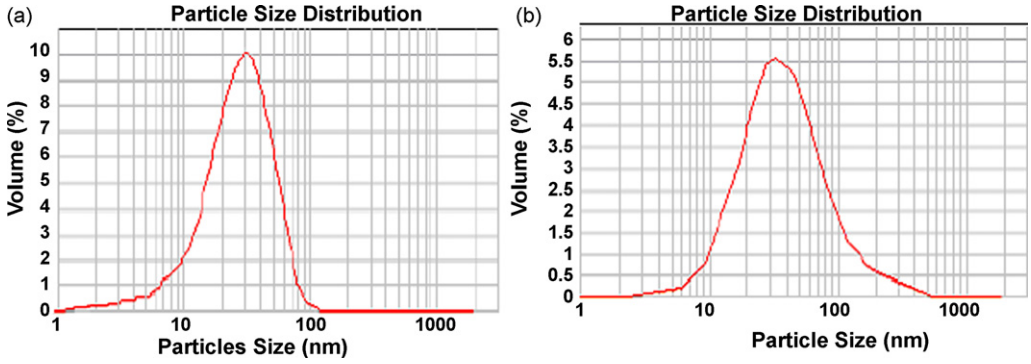

Fig. 3. Particle size distribution of the magnetic Fe_3O_4 particles (a) and KCTS-bound Fe_3O_4 nanoparticles (b).

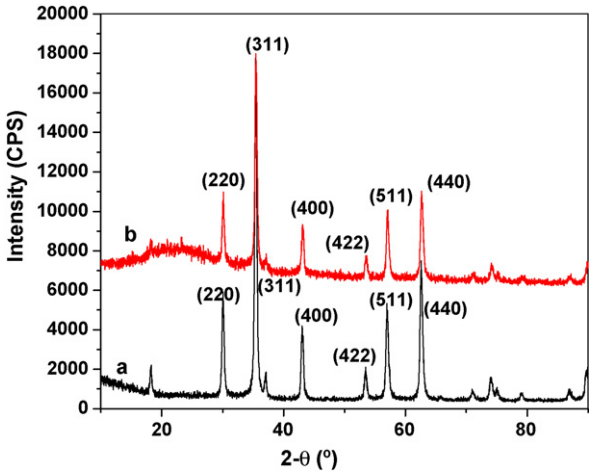

Fig. 4. XRD patterns for the magnetic Fe_3O_4 particles (a) and KCTS-bound Fe_3O_4 nanoparticles (b).

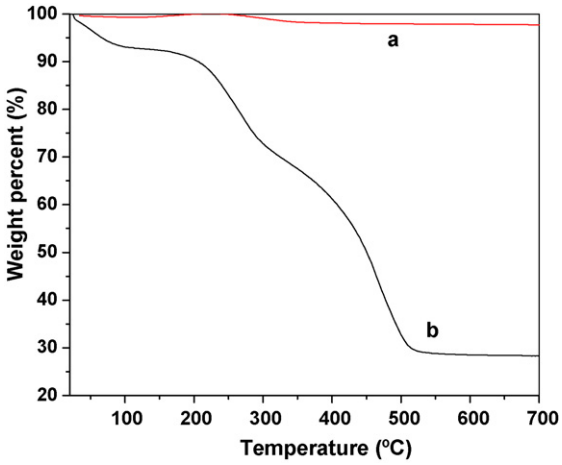

Fig. 5. Thermogravimetric analysis (TGA) of the magnetic Fe_3O_4 particles (a) and KCTS-bound Fe_3O_4 nanoparticles (b).

The broad nature of the diffraction bands in the pattern below is an indication of small particle size, so the particle sizes can be quantitatively evaluated from the XRD data using the Debye–Scherrer equation, which gives a relationship between peak broadening in XRD and particle size.

$$d = \frac{k\lambda}{\beta \cos\theta}$$

In this equation d is the particle size of the crystal, k is the Debye–Scherrer constant (0.89), λ is the X-ray wavelength (0.15406 nm), and β is the line broadening in radian obtained from the full width at half maximum. θ is the Bragg angle. The (3 1 1) crystal in the XRD pattern of the naked Fe_3O_4, β is 0.00658 and θ is 17.78, while for the KCTS-bound Fe_3O_4, β is 0.00569 and θ is 17.71 accordingly. Then we can calculate the diameters of naked Fe_3O_4 and KCTS-bound Fe_3O_4 nanoparticles, which are 21.9 and 25.3 nm, respectively.

3.3. Amount of KCTS bound on Fe_3O_4 nanoparticles

The TGA of the naked and KCTS-bound Fe_3O_4 nanoparticles is shown in Figs. 5 and 6. For naked Fe_3O_4 no significant peak appeared in the DSC curve. Also, the TGA curve shows that the weight loss over the temperature range from 30 to 700 °C is about 2%. This might be due to the loss of residual water in the sample. On the other hand, for KCTS-bound Fe_3O_4, below 200 °C the weight loss of all the nanocomposites is quite small (9.7%) because of the removal of absorbed physical and chemical water. Then the principle chains of KCTS begin to degrade at about 250 °C and the final temperature of decomposition is around 520 °C [20], the weight loss is significant (71.2%). There is no significant weight change from 520 to 700 °C, implying the presence of only iron oxide within the temperature range. The thermochemical behavior described above by the TGA curve was consistent with that indicated by the DSC curve. Accordingly, it revealed that KCTS indeed could be bound to Fe_3O_4 magnetic nanoparticles. From the percentage weight loss in the TGA curve, the amount of KCTS bound on Fe_3O_4 nanoparticles was estimated. The average mass content of KCTS in nanoparticles by TGA was about 61.5%.

To further confirm this binding amount, the carboxyl groups of KCTS on Fe_3O_4 nanoparticles were quantified by the acid–base titration based on the reaction of carboxyl groups of solids and a standardized NaOH. It was found that about 0.0612 mmol of carboxyl groups per 10 mg Fe_3O_4 nanoparticles was available. Accordingly, the quantity of KCTS on Fe_3O_4 nanoparticles could be estimated to be 5.508 mg per 10 mg Fe_3O_4 (there are two carboxyl molecules in a KCTS molecule).

3.4. Magnetic properties of magnetic nanoparticles

Fig. 7 showed a typical magnetization curve of magnetic Fe_3O_4 particles (a) and KCTS-bound Fe_3O_4 magnetic particles (b). As could be seen from Fig. 7, the hysteresis loop showed superparamagnetic property (i.e. no remanence effect), indicating that the single domain magnetic nanoparticles remained in these polymer nanoparticles. The saturation magnetization (σ_s) of the KCTS-bound Fe_3O_4 magnetic microspheres was about

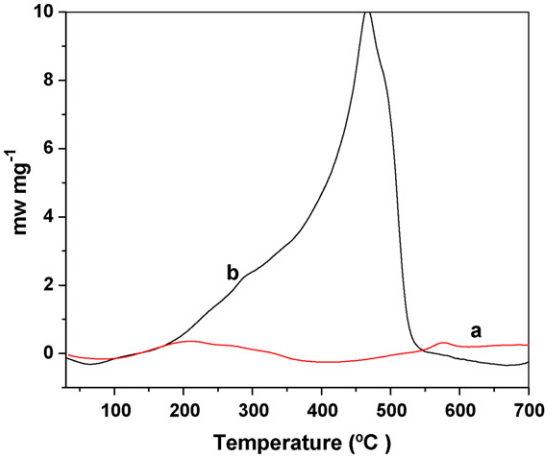

Fig. 6. Differential scanning calorimetry (DSC) analysis of the magnetic Fe_3O_4 particles (a) and KCTS-bound Fe_3O_4 nanoparticles (b).

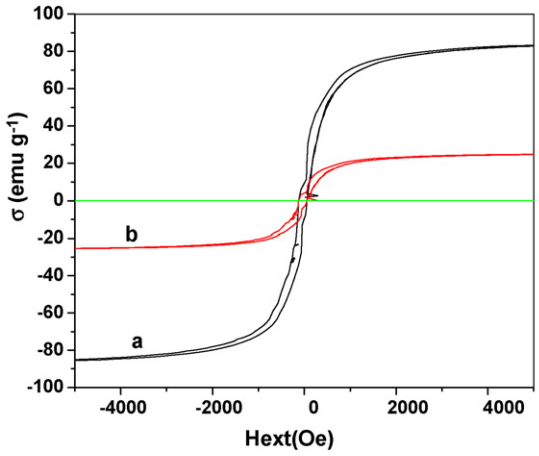

Fig. 7. Hysteresis loop of magnetic Fe_3O_4 particles (a) and KCTS-bound Fe_3O_4 particles (b).

24.8 emu g^{-1} while the pure Fe_3O_4 magnetite nanoparticles was about 83.2 emu g^{-1} in this experiment. Because the weights of all particles used for the measurement of magnetic properties were constant, the decrease of saturation magnetization was due to the increased amount of polymer incorporated in the polymer-coated magnetite suspension. According to some studies suggested that existence of surfactant on the surface of Fe_3O_4 nanoparticles decrease the uniformity due to quenching of surface moments, resulting in the reduction of magnetic moment in such nanoparticles [8]. With a significant fraction of surface atoms, any crystalline disorder within the surface layer may also lead to a significant decrease in the nanoparticle saturation magnetization.

3.5. Stability of magnetic nanoparticles

The stability is one of the most important properties of magnetic nanoparticles. The KCTS-bound Fe_3O_4 magnetic particles were dispersible in water for 5 days. Fig. 8 showed a photograph taken of the KCTS-bound Fe_3O_4 magnetic particles in two separate vials 60 s after a magnet was placed next to one of them.

Fig. 8. Photograph showing the stability of the magnetic nanoparticles dispersion (right vial) and the ready capture of the nanoparticles by a magnet (left vial).

While negligible particle settlement was noticed of the sample on the right, the particles in the left vial were seen essentially quantitatively captured.

20 mg of the KCTS-bound Fe_3O_4 nanoparticles were put in a beaker with 5 ml deionized water under stirring for 48 h, and then dried at 50 °C in a vacuum oven for 12 h. The magnetization of the particles was measured and compared with the original ones. The KCTS-bound Fe_3O_4 magnetic particles have excellent stable performances of magnetization. After stability test, the saturation magnetization (σ_s) of the KCTS-bound Fe_3O_4 magnetic particles was about 23.6 emu g^{-1}, almost the same magnetic property as the original ones (24.8 emu g^{-1}). The magnetic stability feature of the new nanoparticles could ensure the feasible application to liquid separation systems and other areas.

4. Conclusions

A novel KCTS-bound Fe_3O_4 magnetic nanoparticle was fabricated by the binding of KCTS on the surface of Fe_3O_4 nanoparticles via carbodiimide activation. The analyses of TEM and XRD indicated that the KCTS-bound Fe_3O_4 nanoparticles were regular spheres with a mean diameter of 26 nm and the binding of KCTS did not change the spinel structure of Fe_3O_4. The saturated magnetization of composite nanoparticles could reach 24.8 emu g^{-1} and the nanoparticles showed the characteristics of superparamagnetism. The magnetic KCTS-bound Fe_3O_4 nanoparticles have high stability of magnetization. The new nanoparticles may be applied to the magnetic-field assisted drug delivery systems, cell/enzyme immobilization and many other industrial processes.

Acknowledgments

This work was supported by research grants from the National Science Foundation of China (Project No. 20576142), and the National Science Fund for Distinguished Young Scholar of Hunan province of China (No. 06JJ10003).

References

[1] H.W. Gu, K.M. Xu, C.J. Xu, B. Xu, Biofunctional magnetic nanoparticles for protein separation and pathogen detection, Chem. Commun. (2006) 941–949.
[2] E. Katz, I. Willner, Magnetic control of electrocatalytic and bioelectrocatalytic processes, Angew. Chem. Int. Ed. 42 (2003) 4576–4588.
[3] Y.S. Kang, S. Risbud, J.F. Rabolt, P. Stroeve, Synthesis and characterization of nanometer-size Fe_3O_4 and γ-Fe_2O_3 particles, Chem. Mater. 8 (1996) 2209–2212.
[4] K. Woo, J. Hong, S. Choi, H. Lee, J. Ahn, C.S. Kim, S.W. Lee, Easy synthesis and magnetic properties of iron oxide nanoparticles, Chem. Mater. 16 (2004) 2814–3218.
[5] K.S. Suslick, M. Fang, T. Hyeon, Sonochemical synthesis of iron colloids, J. Am. Chem. Soc. 118 (1996) 11960–11961.
[6] S. Santra, R. Tapec, N. Theodoropoulou, J. Dobson, A. Hebard, W.H. Tan, Synthesis and characterization of silica-coated iron oxide nanoparticles in microemulsion: the effect of nonionic surfactants, Langmuir 17 (2001) 2900–2906.
[7] M. Mikhaylova, D.K. Kim, N. Bobrysheva, M. Osmolowsky, V. Semenov, T. Tsakalakos, M. Muhammed, Superparamagnetism of mag-

netite nanoparticles: dependence on surface modification, Langmuir 20 (2004) 2472–2477.

[8] S.R. Wa, J.S. Huang, H.S. Yan, Size-controlled preparation of magnetite nanoparticles in the presence of graft copolymers, J. Mater. Chem. 16 (2006) 298–303.

[9] D.H. Kim, S.H. Lee, K.H. Im, K.N. Kim, K.M. Kim, I.B. Shim, M.H. Lee, Y.K. Lee, Surface-modified magnetite nanoparticles for hyperthermia: preparation, characterization, and cytotoxicity studies, Curr. Appl. Phys. 6S1 (2006) e242–e246.

[10] P. Wunderbaldinger, L. Josephson, R. Weissleder, Tat peptide directs enhanced clearance and hepatic permeability of magnetic nanoparticles, Bioconjugate Chem. 13 (2002) 264.

[11] Y.L. Ting, H.H. Shang, H.H. Sheng, P.T. Szu, S.Y. Chen, Preparation and characterization of thermal-sensitive ferrofluids for drug delivery application, J. Magn. Magn. Mater. 310 (2007) 2850–2852.

[12] C. Alexiou, W.G. Arnold, H. Peter, J.K. Roswitha, R. Helmut, G.P. Fritz, B. Christian, S.L. Andreas, Magnetic mitoxantrone nanoparticle detection by histology X-ray and MRI after magnetic tumor targeting, J. Magn. Magn. Mater. 225 (2001) 187–193.

[13] W. Wang, L. Deng, Z.H. Peng, X. Xiao, Study of epoxydized magnetic hydroxyl particles as a carrier for immobilizing penicillin G acylase, Enzyme Microb. Technol. 40 (2007) 255–261.

[14] P. Ding, K.L. Huang, G.Y. Li, Kinetics of adsorption of Zn(II) ion on chitosan derivatives, Int. J. Biol. Macromol. 39 (2006) 222–227.

[15] Y.C. Chang, D.H. Chen, Preparation and adsorption properties of monodisperse chitosan-bound Fe_3O_4 magnetic nanoparticles for removal of Cu(II) ions, J. Colloid Interface Sci. 283 (2005) 446–451.

[16] E.H. Kima, Y. Ahnb, H.S. Lee, Biomedical applications of superparamagnetic iron oxide nanoparticles encapsulated within chitosan, J. Alloys Compd. 434/435 (2007) 633–636.

[17] L.M. Zhou, Y.P. Wang, Z.R. Liu, Q.W. Huang, Carboxymethyl chitosan-Fe3O4 nanoparticles: preparation and adsorption behavior toward Zn^{2+} ions, Acta Physico-Chim. Sinica 22 (2006) 1342–1346.

[18] Y.C. Chang, D.H. Chen, Adsorption kinetics and thermodynamics of acid dyes on a carboxymethylated chitosan-conjugated magnetic nano-adsorbent, Macromol. Biosci. 5 (2005) 254–261.

[19] Y. Wu, J. Guo, W.L. Yang, C.C. Wang, S.K. Fu, Preparation and characterization of chitosan–poly (acrylic acid) polymer magnetic microspheres, Polymer 47 (2006) 5287–5294.

[20] J. Zhi, Y.J. Wang, Y.C. Lu, J.Y. Ma, G.S. Luo, In situ preparation of magnetic chitosan/Fe3O4 composite nanoparticles in tiny pools of water-in-oil microemulsion, React. Funct. Polym. 66 (2006) 1552–1558.